

EFFECT OF FATIGUE PRE-LOADING ON MIXED-MODE STRESS-CORROSION CRACKING IN HIGH-STRENGTH STEEL

J. Toribio, E. Ovejero and V. Kharin

Department of Materials Science, University of La Coruña,
ETSI Caminos, Campus de Elviña, 15192 La Coruña, Spain

ABSTRACT

This work describes experimental evidence of mixed-mode stress-corrosion cracking of high-strength steel and discusses the role of cyclic load history. To this end, finite deformation analysis of a plane strain crack subjected to mode I loading under small scale yielding was performed and different continuum mechanics variables analyzed throughout the pre-loading route, in particular the *equivalent plastic strain* as a measure of mechanical damage. Results of the computational elastoplastic analysis of stress-strain evolution in the vicinity of the crack tip subjected to fatigue and subsequent rising loading are consistent with the experimental fact of anisotropic cracking behaviour of prestressing steel in corrosive environment. It can explain (if coupled with the inherent anisotropy associated with the oriented microstructure of the steel) why crack branching takes place at a deflection angle in relation to mode I crack extension.

INTRODUCTION

Fatigue pre-cracking is a very common and useful crack generating technique for posterior stress corrosion testing. However, it has been documented many times that fatigue pre-loading substantially alters the results from stress-corrosion cracking tests in different aggressive environments (cf. [1,2]), so that the role of cyclic pre-loading in environmentally assisted fracture is far from being totally understood.

This work describes experimental evidence of mixed-mode stress-corrosion cracking of high-strength cold drawn steel and discusses the role of cyclic load history, in addition to the inherent strength anisotropy of the material as a consequence of the oriented pearlitic microstructure after the steelmaking process by means of very heavy drawing [3,4].

EXPERIMENTAL PROCEDURE

The material used is a cold drawn prestressing steel wire whose chemical composition and mechanical properties are given in Tables 1 and 2. Metallographic techniques [5,6] were used to reveal the fine pearlitic microstructure of the steel. Figs.1 and 2 show micrographs of the longitudinal section at the two basic microstructural levels of pearlitic colonies and lamellae. Both microstructural units are seen to be markedly oriented in a direction parallel or quasi-parallel to the wire axis or cold drawing direction.

TABLE 1
CHEMICAL COMPOSITION (wt %) OF THE STEEL

C	Mn	Si	P	S	Cr	V	Al
0.80	0.69	0.23	0.012	0.009	0.265	0.060	0.004

TABLE 2
MECHANICAL PROPERTIES OF THE STEEL

Young's Modulus (GPa)	Yield Strength (MPa)	UTS (MPa)	Elongation under UTS (%)	Ramberg-Osgood* P (MPa)	n
199	1500	1760	5.0	2576	11.49

* Ramberg-Osgood stress-strain curve $\epsilon = \sigma/E + (\sigma/P)^n$



Figure 1: Optical micrograph of the longitudinal metallographic section showing the first microstructural level, i.e., the pearlite colonies oriented after cold drawing (vertical side: wire axis or cold drawing direction).

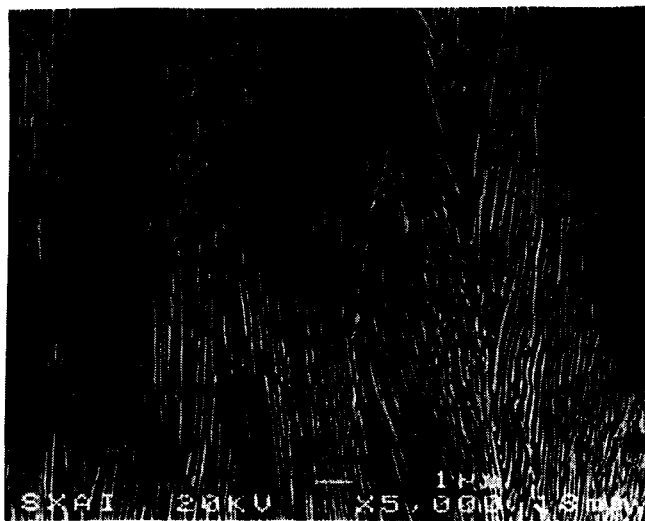


Figure 2: Scanning electron micrograph of the longitudinal metallographic section showing the second microstructural level, i.e., the pearlitic lamellar microstructure oriented after cold drawing (vertical side: wire axis or cold drawing direction).

Slow strain rate tests were performed on transversely precracked rods immersed in aqueous environment. Specimens were precracked by axial fatigue in air with a maximum cyclic stress intensity factor at the final phase $K_{max} = 0.30K_{IC}$, where $K_{IC} = 107 \text{ MPam}^{1/2}$ is the fracture toughness. An aqueous solution of 1 g/l

$\text{Ca(OH)}_2 + 0.1 \text{ g/l NaCl}$ (pH=12.5) was used. Tests were conducted at a crosshead speed of $1.7 \times 10^{-3} \text{ mm/min}$ and at a constant electrochemical potential $E = -600 \text{ mV SCE}$ (anodic), so the mechanism of environment-sensitive fracture must be *localised anodic dissolution* (LAD) [1,7].

The main result of the stress-corrosion cracking (SCC) tests is a special *fracture profile* (Fig. 3) associated with the anisotropic behaviour of the cold drawn steel wire. Cracking from the tip of the mode I fatigue pre-crack develops initially in mode I and later at an angle about 75° to its plane, thus producing mixed mode propagation. In addition, another crack embryo (a second kink) exists symmetrically to the pre-crack, i.e., the phenomenon is initially crack branching (two crack embryos) and finally crack deflection, that is, only one of them becomes the final fracture path.

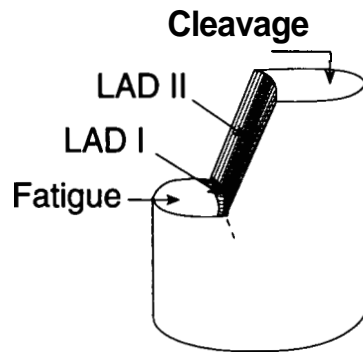


Figure 3: Aspect of the fracture profile in the SCC test showing subcritical (slow) crack growth by localized anodic dissolution in mode I (LAD I) and mixed-mode with a strong mode II component (LAD II).

A fractographic analysis was performed by scanning electron microscopy. Figs. 4 shows the microscopic fracture modes associated with the subcritical crack growth area LAD I (before crack branching). The general appearance of the topography LAD I is similar to the micro-void coalescence (MVC) fracture mode in the same steel in air, although the former is produced by metal dissolution.



Figure 4: Scanning electron micrograph of the subcritical crack growth area LAD I (before crack branching).

Figs. 5 shows the microscopic fracture modes associated with the subcritical crack growth area LAD II (after crack deflection). As in the previous case, this topography is also similar to MVC, although in this case there is a kind of *enlargement* or *orientation* of the micro-fracture units along the propagation direction which is quasi-parallel to the cold drawing axis (after crack deflection).

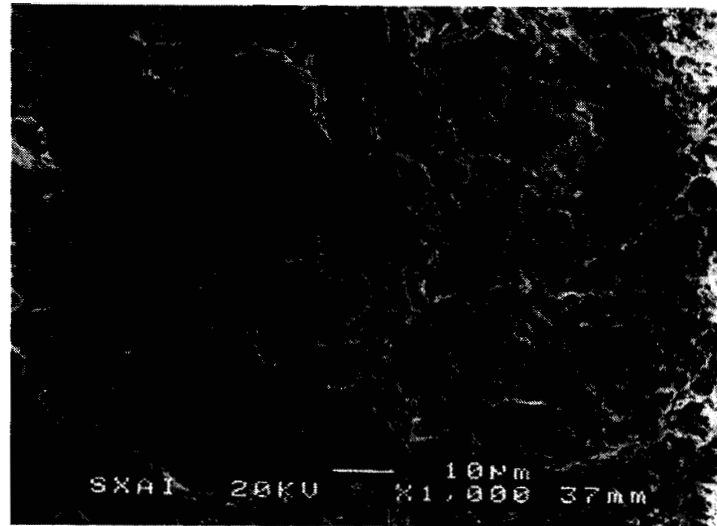


Figure 5: Scanning electron micrograph of the subcritical crack growth area LAD II (after crack deflection).

Fig. 6 shows the microscopic appearance of the crack branching area, i.e., the separation (discontinuity) between the two zones LAD I and LAD II. Some cleavage facets may be observed near such a separation, which indicates that fast fracture is locally produced at the moment of crack branching, probably because the macroscopic crack reaches a point with local pre-damage produced by cold drawing.

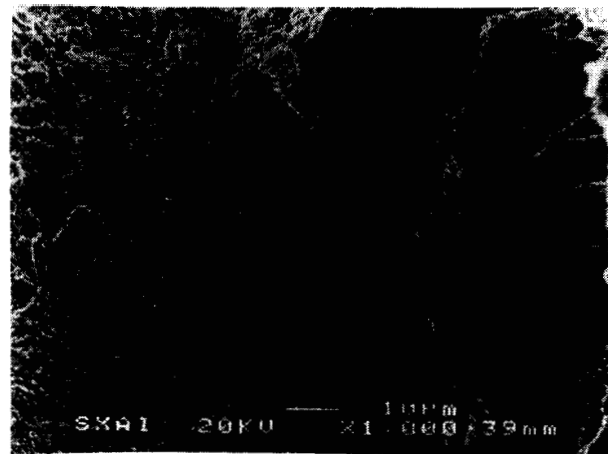


Figure 6: Scanning electron micrograph of the crack branching area, i.e., the separation (discontinuity) between the two zones LAD I and LAD II, showing some cleavage facets near such a separation.

The primary reason for this crack deviation is the very oriented pearlitic microstructure of the steel (cf. [8]) producing strength anisotropy. However, fatigue pre-cracking could be an additional factor contributing to crack deflection due to the special distribution of variables (stresses and strains) in the vicinity of a crack tip subjected to repetitive cyclic loading, as discussed in the following section of the paper.

NUMERICAL MODELLING

In this paper the effect of fatigue precracking is analyzed by numerical modelling of the stress-strain state near the crack tip under plane-strain small-scale yielding in an elastoplastic material with kinematic strain-hardening whose characteristics correspond to the steel used in the experimental programme (cf. Table 2). The crack was modelled as a round-tip slit with initial height (twice the tip radius) of 2.5 μm in agreement with experimental

data for fatigue cracks in high-strength steels [9]. The loading history consisted of several (up to ten) zero-to-tension cycles according to the final phase of the experimental fatigue programme with $K_{\max} = 32 \text{ MPam}^{1/2}$ ($0.30K_{IC}$) followed by rising load corresponding to the slow strain rate testing. The nonlinear finite element code MARC [10] was employed with updated Lagrangian formulation.

Attention was paid to the patterns of evolution of the following macroscopic (continuum mechanics) variables closely related to environmentally assisted cracking in general and localised anodic dissolution as an important particular case:

- (i) *Equivalent plastic strain* as a measure of mechanical pre-damage [11] which produces a more disordered material structure therein before stress corrosion cracking and enhances posterior localised anodic dissolution in the near-tip area. In a coupled way, it has been shown that anodic dissolution enhances crack tip deformation [12-15].
- (ii) *Equivalent plastic strain rate* responsible for the dynamic phenomenon of passive film rupture due to the deformation itself. In addition, this variable also governs hydrogen transport by moving dislocations in the plastic zone [16,17] and it is known [18,19] that, even at anodic potentials, hydrogen may be present in the critical area as a consequence of the *local* electrochemical conditions near the crack tip.
- (iii) *Hydrostatic stress* as the macroscopic variable governing hydrogen transport by a mechanism of random-walk stress-assisted diffusion [20,21], according to which hydrogen (present in the near-tip area due to the local electrochemical conditions) diffuses towards the points of maximum hydrostatic stress, so that it is driven by the *gradient* of this variable.

The listed governing variables were studied at monotonic rising loading after fatigue to reproduce the slow strain rate tests. However, as described in the experimental results, there is a certain subcritical crack growth in mode I (LAD I) before crack deflection takes place. This means that the numerical analysis of the continuum mechanics variables (performed after loading/unloading the specimen to simulate fatigue pre-cracking) gives the stress-strain state in the vicinity of the deformed crack tip *without* considering subcritical crack extension by stress corrosion cracking, i.e., neglecting the stress-strain redistribution as a consequence of the crack growth in mode I. This hypothesis seems to be adequate, since the mode I propagation distance is about 150 μm , i.e., less than 10% of the macroscopic crack length.

DISCUSSION

The distribution of equivalent plastic strain at a reference stress intensity factor $K_r = 0.44K_{IC} > K_{\max}$ (K_{\max} is the maximum during the last stage of fatigue precracking) is given in Fig. 7 in the deformed configuration of the near-tip domain (the crack plane being the x-axis and the load applied in the y-direction). A vertex is observed on the tip profile with secondary peaks of equivalent plastic strain out of the crack plane. Two localized shear bands emerge from the vertex, one of them very close to the drawing direction and markedly deviated from the precrack line. The formation of this band as the easier fracture path by localised anodic dissolution (or pure stress corrosion cracking), in combination with the strength anisotropy of the oriented microstructure (weakness in the wire axis or cold drawing direction), is consistent with crack kinking in the stress corrosion cracking tests.

Fig. 8 displays the distribution of equivalent plastic strain rate for rising load after precracking (at $K_r = 0.44 K_{IC} > K_{\max}$). One of the bands of fast plastic straining (and associated passive film rupture and dislocation motion) is approximately located along an 80°-direction from the initial crack plane. This indicates the preferred direction of film rupture and further localised anodic dissolution along the newly created fresh surface. This 80°-direction also signals the preferred path for hydrogen transport by dislocational dragging as the plastic zone spreads. Both phenomena of plasticity-dissolution interactions, in addition to the weakening in this direction produced by microstructural orientation, represent two more reasons for crack deflection in agreement with the experimental cracking profile shown in Fig. 3.

Fig. 9 shows the distribution of hydrostatic stress for rising loading after fatigue cycling (at $K_r = 0.44 K_{IC} > K_{\max}$). The closeness of the iso-lines suggests that the maximum hydrostatic stress gradient which drives stress-assisted hydrogen diffusion is achieved outside the initial crack plane. The ridge of the relief of hydrostatic stress follows a direction of 45 to 80° to the mode I plane and this indicates the area of fastest hydrogen accumulation. Hydrogen is driven in the directions of the arrows (elevated hydrostatic stress gradients and accelerated hydrogen flux) rather than ahead of the crack tip (along x-axis) where the flux is even delayed by the local drop of hydrostatic stress. This facilitates crack deflection and is consistent with the experienced stress corrosion cracking path shown in Fig. 3.

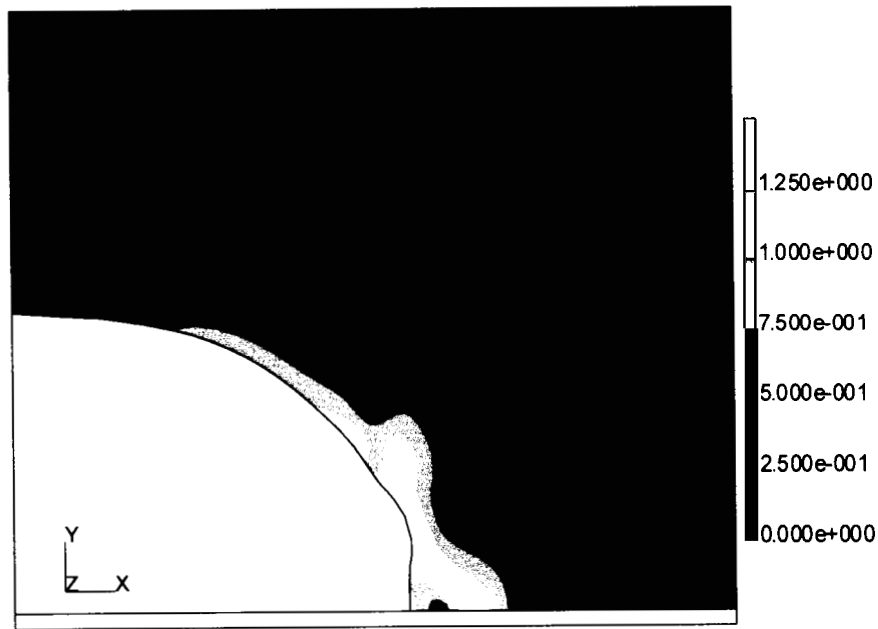


Figure 7: Distribution of equivalent plastic strain (arbitrary units) near the deformed crack tip at $K_I = 0.44 K_{IC}$ in a slow strain rate test after fatigue cycling with $K_{max} = 0.30 K_{IC}$.

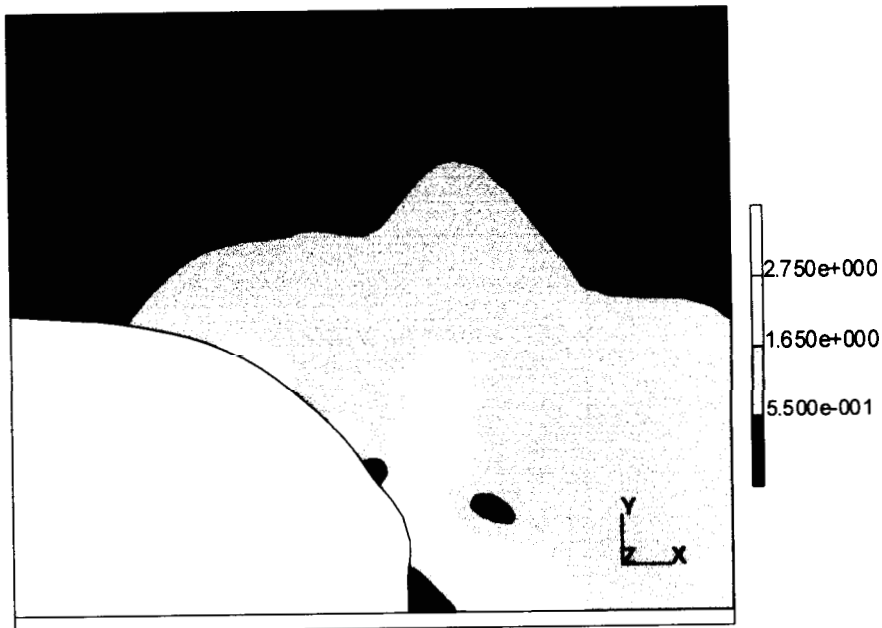


Figure 8: Distribution of equivalent plastic strain rate (arbitrary units) near the deformed crack tip at $K_I = 0.44 K_{IC}$ in a slow strain rate test after fatigue cycling with $K_{max} = 0.30 K_{IC}$.

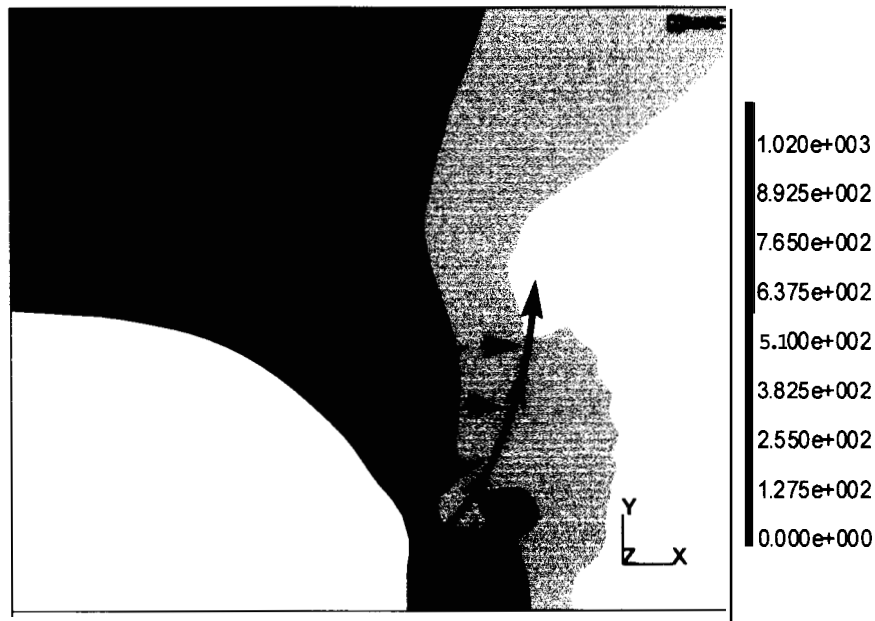


Figure 9: Distribution of hydrostatic stress (arbitrary units) near the deformed crack tip at $K_I = 0.44 K_{IC}$ in a slow strain rate test after fatigue cycling with $K_{max} = 0.30 K_{IC}$; bold line shows the ridge of the hydrostatic stress relief and arrows mark hydrostatic stress gradients and corresponding directions of accelerated hydrogen flux near the crack tip.

CONCLUSION

Results of the computational elastoplastic analysis are consistent with the experimental fact of anisotropic stress-corrosion cracking behaviour of prestressing steel. This explains, in addition to the inherent anisotropy associated with the oriented microstructure of the steel, why crack branching takes place at a deflection angle of about 75° in the case of stress corrosion cracking by localised anodic dissolution.

Acknowledgement

Financial support of this work by the Spanish CICYT (Grant MAT97-0442) and *Xunta de Galicia* (Grant XUGA 11802B97) is gratefully acknowledged. In addition, the authors wish to express their gratitude to EMESA TREFILERIA S.A. (La Coruña, Spain) for providing the steel used in the experimental programme.

REFERENCES

1. Toribio, J., Lancha, A.M. and Elices, M. (1993) *Corros. Sci.* **35**, 521.
2. Toribio, J. and Kharin, V. (1997) *Mater. & Design* **18**, 87.
3. Langford, G. (1970) *Metall. Trans.* **1**, 465.
4. Embury, J.D. and Fisher, R.M. (1966) *Acta Metall.* **14**, 147.
5. Samuels, L.E. (1992). *Optical Microscopy of Carbon Steels*, ASM, Metals Park, Ohio.
6. Vander Voort, G.F. (1984). *Metallography. Principles and Practice*, McGraw-Hill Inc., New York.
7. Parkins, R.N., Elices, M., Sánchez-Gálvez, V. and Caballero, L. (1982) *Corros. Sci.* **22**, 379.
8. Toribio, J. and Ovejero, E. (1998) *Mech. Time-Dependent Mater.* **1**, 307.
9. Handerhan, K.J. and Garrison Jr., W.M. (1992) *Acta Metall. Mater.* **40**, 1337.
10. MARC User Information (1994). Marc Analysis Research Corporation, Palo Alto.
11. Suresh, S. (1991). *Fatigue of Materials*, Cambridge University Press, Cambridge.
12. Revie, R.W. and Uhlig, H.H. (1972) *Corros. Sci.* **12**, 669.
13. Kramer, I.R. (1974) *Scripta Metall.* **8**, 1231.

14. Uhlig, **H.H.** (1981) *Corros. Sci.* **21**, 159.
15. Wei, **X.**, Li, J., Zhou, X. and Ke, **W.** (1996) *Corros. Sci.* **38**, 989.
16. Tien, J.K., Thompson, A.W., Bernstein, I.M. and Richards, R.J. (1976) *Metall. Trans.* **7A**, 821.
17. Nair, S.V., Jensen, R.R. and Tien, J.K. (1983) *Metall. Trans.* **14A**, 385.
18. Barth, C.F., Steigerwald, E.A. and Troiano, A.R. (1969) *Corrosion-NACE* **25**, 353.
19. Smith, J.A., Peterson, **M.H.** and Brown, B.F. (1970) *Corrosion-NACE* **26**, 539.
- 20.** Van Leeuwen, **H.P.** (1974) *Engng. Fracture Mech.* **6**, 141.
21. Toribio, J. and Kharin, V. (1997) *Fatigue Fracture Engng. Mater. Structures* **20**, 729.